JOURNAL OF Materials CHEMISTRY

Two new diamine templated lanthanum sulfates, $La_2(H_2O)_2(C_4H_{12}N_2)(SO_4)_4$ and $La_2(H_2O)_2(C_2H_{10}N_2)_3(SO_4)_6 \cdot 4H_2O$, with 3D and 2D crystal structures

Thierry Bataille and Daniel Louër*

Laboratoire de Chimie du Solide et Inorganique Moléculaire, UMR 6511 CNRS, Institut de Chimie, Université de Rennes I, Avenue du Général Leclerc, 35042 Rennes Cedex, France. E-mail: Daniel.Louer@univ-rennes1.fr

Received 23rd July 2002, Accepted 24th September 2002
First published as an Advance Article on the web 23rd October 2002

Two new lanthanum sulfates have been synthesised under hydrothermal conditions in the presence of piperazine or ethylenediamine. The compounds have been structurally characterised from single-crystal X-ray diffraction. $La_2(H_2O)_2(C_4H_{12}N_2)_2(SO_4)_4$, **1**, and $La_2(H_2O)_2(C_2H_{10}N_2)_3(SO_4)_6 \cdot 4H_2O$, **2**, crystallise with monoclinic symmetry, space group $P2_1/c$. Compound **1** exhibits a three-dimensional anionic open-framework constituted by lanthanum atoms and sulfate groups. The charge compensation is ensured by the presence of piperazinium cations occluded in the cavities of the structure. Compound **2** has a layered structure, built from inorganic anionic sheets of lanthanum sulfates between which are located the ethylenediammonium cations and water molecules. The thermal behaviour of the two compounds has been studied by temperature-dependent powder X-ray diffraction and thermal analyses. Intermediates have been characterised during the dehydration stages. The decomposition temperature of the diamines is also discussed with regard to their hydrogen bonding to the framework. The products obtained at the final stages of the decomposition are $La_2(SO_4)_3$ and $La_2O_2SO_4$.

Introduction

Recent research on the synthesis of new compounds possessing inorganic open frameworks with guest organic entities has revealed the diversity of such materials in terms of structure topology and composition, particularly in the presence of organic amines as templates.[1,2] In these materials, the phosphate anion has often been involved as a $[TO_4]$ unit (T = tetrahedrally coordinated element) in the formation of the inorganic framework,[3,4] though compounds based on other tetrahedral groups, such as germanate[5,6] and arsenate,[7] have also been reported. Frameworks containing sulfate anions have been considerably less investigated. This is surprising since sulfates are known to promote a diversity of structural arrangements in inorganic solids.[8] Representative examples are the six compounds identified in the cadmium hydroxide sulfate family, including three polymorphs of $Cd_2(OH)_2SO_4$,[9] and the five lanthanum ammonium sulfates,[10–14] including two polymorphs of $La(NH_4)(SO_4)_2$, both families display three- and two-dimensional crystal structures. This versatile behaviour of the sulfate group in inorganic frameworks, combined with the known role of organic amines as templates, has motivated the present investigation of lanthanum sulfate derivatives. The possibility of synthesising novel amine templated phases is reinforced by the formation, in the presence of amine, of sulfate-containing open structures with zinc,[15] cadmium[16] and scandium,[17] and by recent studies having shown the comparable structure-directing role of ammonium and amines. For example, recently our group reported the crystal structure of an ammonium tin oxalate,[18] which displays structural similarities with amine-templated tin oxalates,[19] and new ammonium and ethylenediamine cadmium zirconium oxalates with both helical structures.[20] Furthermore, it should be noted that the flexibility of lanthanum atom coordination (from seven- to twelve-fold) can also be an aid to the formation of new amine-based compounds. This study deals with the synthesis, under mild hydrothermal conditions, the structure determination and the thermal behaviour of two new lanthanum sulfates templated by piperazine and ethylenediamine.

Experimental

Synthesis

Lanthanum piperazinium sulfate, $La_2(H_2O)_2(C_4H_{12}N_2)(SO_4)_4$, **1**, was synthesised hydrothermally from $La_2(SO_4)_3 \cdot 8H_2O$ (0.7 mmol), piperazine hexahydrate (2 mmol), concentrated sulfuric acid (0.5 ml) and distilled water (7 ml) in the molar ratio La : amine : SO_4 : H_2O = 2 : 3 : 13 : 555 (pH = 1). The homogeneous mixture was sealed in a 23 ml Teflon-lined acid digestion bomb (Parr) and heated at 423 K for 24 h. Aggregates of colourless platy crystals were obtained as a single product. Lanthanum ethylenediammonium sulfate, $La_2(H_2O)_2(C_2H_{10}N_2)_3(SO_4)_6 \cdot 4H_2O$, **2**, was prepared in the same way from a starting mixture of $La_2(SO_4)_3 \cdot 8H_2O$ (0.7 mmol), ethylenediamine 99% (4.4 mmol), concentrated sulfuric acid (0.25 ml) and distilled water (5 ml) in the molar ratio La : amine : SO_4 : H_2O = 2 : 6 : 9 : 397 (pH = 8). After heating at 423 K for 4 d, small colourless needles were obtained quantitatively. The pHs of the solutions were unchanged after reaction. The chemical formulae of the two phases were deduced from the crystal structure determination from single-crystal X-ray diffraction data and thermal analyses.

Single-crystal data collection and structure determination

Suitable crystals of **1** and **2** were glued to a glass fibre mounted on a four-circle Nonius Kappa CCD area-detector diffractometer. Intensity data sets were collected using Mo Kα radiation (λ = 0.71073 Å) through the program COLLECT.[21] Correction for Lorentz-polarisation effect, peak integration

DOI: 10.1039/b207212m

Table 1 Crystallographic data for $La_2(H_2O)_2(C_4H_{12}N_2)(SO_4)_4$, **1**, and $La_2(H_2O)_2(C_2H_{10}N_2)_3(SO_4)_6{\cdot}4H_2O$, **2**

	1	**2**
Empirical formula	$C_4H_{16}La_2N_2O_{18}S_4$	$C_6H_{42}La_2N_6O_{30}S_6$
Formula weight/g mol^{-1}	786.25	1148.64
Crystal system	Monoclinic	Monoclinic
Space group	$P2_1/c$ (no. 14)	$P2_1/c$ (no. 14)
a/Å	16.7936(2)	6.6605(1)
b/Å	9.5858(1)	26.7013(6)
c/Å	22.5827(3)	10.0256(3)
β/°	104.2164(4)	104.874(1)
V/Å^3	3524.03(7)	1723.25(7)
Z	8	2
ρ_{calc}/g cm^{-1}	2.964	2.214
Crystal size/mm^3	0.25 × 0.18 × 0.04	0.53 × 0.05 × 0.03
λ (Mo Kα)/Å	0.71073	0.71073
μ/mm^{-1}	5.359	2.922
θ range/°	1.00–32.03	1.00–27.48
Index range	$-22 \leqslant h \leqslant 25$	$-8 \leqslant h \leqslant 8$
	$-13 \leqslant k \leqslant 14$	$-34 \leqslant k \leqslant 29$
	$-32 \leqslant l \leqslant 33$	$-13 \leqslant l \leqslant 12$
Unique data	12271	3953
Observed data $[I > 2\sigma(I)]$	8634	2555
R_{int}	0.0637	0.0897
Refinement method	Full matrix least-squares on $\|F^2\|$	Full matrix least-squares on $\|F^2\|$
R_1 $[I > 2\sigma(I)]$	0.0430	0.0426
R_1 (all data)	0.0752	0.0919
ωR_2 $[I > 2\sigma(I)]$	0.0970	0.0744
ωR_2 (all data)	0.1144	0.0882
GoF	1.068	0.988
No. of variables	572	311
No. of constraints	24	21
Largest difference map peak and hole/e Å^{-3}	2.88 and −2.05	1.62 and −1.00

and background determination was carried out with the program DENZO.[22] Frame scaling and unit cell parameter refinement were performed with the program SCALEPACK.[22] Numerical absorption correction was performed by modelling the crystal faces using NUMABS.[23] Crystallographic data are listed in Table 1.

Both structures were solved in the monoclinic symmetry, space group $P2_1/c$ (no. 14). Lanthanum atoms, sulfate groups and organic moieties were located using direct methods with the program SIR97.[24] The remaining non-hydrogen atoms were found from successive Fourier calculations using SHELXL-97.[25] For compound **1**, the hydrogen atoms of the piperazinium cations were generated by assuming a tetrahedral hybridisation for both carbon and nitrogen atoms, and refined using the 'riding' option available in SHELXL-97. The hydrogen atoms of the water molecules were located on the Fourier maps and the distances to their oxygen atoms were constrained to 0.96(12) Å. H–H distances were also constrained to 1.550(25) Å, so that the H–O–H angles fitted the ideal value of a tetrahedral angle. Large values of the anisotropic U_{11} component of the atomic displacement parameter were observed for two oxygens, O33 and O34, *i.e.* about 0.36 Å^2 for each. Their positions were split subsequently and the anisotropic displacement parameters for the split atoms were restrained to be refined with the same values. For compound **2**, all the H atoms were located by Fourier syntheses. N–H, C–H and O–H distances were constrained to be equal to 0.98(2), 0.97(2) and 0.96(2) Å, respectively. Results of the least-squares structure refinements are given in Table 1. Selected bond distances and angles, as well as hydrogen bonds, are listed in Tables 2 and 3 for **1** and Tables 4 and 5 for **2**.

CCDC reference numbers 183663 and 190425.

See http://www.rsc.org/suppdata/jm/b2/b207212m/ for crystallographic data in CIF or other electronic format.

Table 2 Selected bond distances (Å) and angles (°) in $La_2(H_2O)_2(C_4H_{12}N_2)(SO_4)_4$, **1**

Within La polyhedra[a]			
La1–O21^{I}	2.772(3)	La2–O12	2.466(4)
La1–O24	2.790(4)	La2–O22	2.513(3)
La1–O44	2.555(4)	La2–O23^{III}	2.881(3)
La1–O51^{II}	2.740(4)	La2–O31	2.436(3)
La1–O52	2.597(3)	La2–O63	2.561(3)
La1–O53	2.672(3)	La2–O64	2.620(3)
La1–O54	2.631(4)	La2–O71^{IV}	2.515(3)
La1–O62	2.569(3)	La2–O74^{IV}	2.709(3)
La1–O72	2.586(3)	La2–O83	2.649(4)
La1–O73	2.634(3)		
La3–O13	2.502(4)	La4–O11	2.486(4)
La3–O14^{V}	2.497(3)	La4–O21^{I}	2.654(3)
La3–O32^{VI}	2.482(4)	La4–O23	2.609(3)
La3–O33A	2.431(7)	La4–O34A^{I}	2.591(7)
La3–O33B	2.441(8)	La4–O34B^{I}	2.475(7)
La3–O41^{VII}	2.510(4)	La4–O42	2.485(4)
La3–O83	2.695(4)	La4–O61	2.574(4)
La3–O84	2.609(3)	La4–O81^{I}	2.530(4)
La3–Ow31	2.592(4)	La4–Ow41	2.648(3)
La3–Ow32	2.634(9)	La4–Ow42	2.550(4)
Within piperazinium ions			
C11–N12	1.446(8)	N12–C11–C16	113.6(5)
C11–C16	1.466(8)	C11–N12–C13	115.9(6)
N12–C13	1.448(9)	N12–C13–C14	115.4(6)
C13–C14	1.463(8)	C13–C14–N15	111.9(5)
C14–N15	1.467(8)	C16–N15–C14	114.2(5)
N15–C16	1.463(8)	N15–C16–C11	113.4(5)
C21–N26	1.460(8)	N26–C21–C22	112.0(6)
C21–C22	1.472(9)	C21–C22–N23	112.3(5)
C22–N23	1.491(8)	C24–N23–C22	112.6(5)
N23–C24	1.451(8)	N23–C24–C25	113.6(6)
C24–C25	1.522(9)	N26–C25–C24	109.7(5)
C25–N26	1.504(8)	C21–N26–C25	110.9(5)

[a]Symmetry codes: I, x, $-1 + y$, z; II, $1 - x$, $\frac{1}{2} + y$, $\frac{1}{2} - z$; III, x, $1 + y$, z; IV, $1 - x$, $1 - y$, $-z$; V, $2 - x$, $1 - y$, $-z$; VI, $2 - x$, $2 - y$, $-z$; VII, $2 - x$, $\frac{1}{2} + y$, $\frac{1}{2} - z$.

In situ powder X-ray diffraction

Powder diffraction data of intermediate phases observed during the thermal decomposition of compounds **1** and **2** were collected *in situ* with a Bruker D5005 diffractometer, using Cu Kα radiation (λ(Kα_1) = 1.5406 Å, λ(Kα_2) = 1.5444 Å)

Table 3 Possible hydrogen bonds (Å) in $La_2(H_2O)_2(C_4H_{12}N_2)(SO_4)_4$, **1**

D–H···A[a]	d(D–H)	d(H···A)	d(D···A)	∠D–H···A/°
N12–H12A···O61	0.99	2.53	3.386(9)	144.2
N12–H12B···O74^{I}	0.99	2.08	3.043(8)	164.0
N12–H12B···O63	0.99	2.34	2.873(7)	112.7
N15–H15A···O54^{II}	0.99	2.11	3.075(8)	163.6
N15–H15B···O73^{III}	0.99	2.05	2.988(6)	157.0
N15–H15B···O52^{III}	0.99	2.51	3.031(7)	112.6
N23–H23A···O43	0.99	2.20	2.752(6)	114.1
N23–H23A···O64	0.99	2.52	3.243(7)	129.9
N23–H23B···O53	0.99	2.06	3.005(7)	158.1
N23–H23B···O62	0.99	2.57	3.193(7)	121.3
N26–H26A···O14^{IV}	0.99	2.31	3.123(7)	138.8
N26–H26B···O74^{V}	0.99	2.14	3.037(7)	149.5
Ow31–H31A···Ow41	0.958(12)	1.92(2)	2.850(5)	164(6)
Ow31–H31B···O42^{VI}	0.951(12)	1.98(3)	2.812(5)	145(5)
Ow32–H32A···O13^{VII}	0.969(12)	2.00(9)	2.725(10)	130(10)
Ow32–H32B···O34A^{VIII}	0.972(12)	2.40(13)	3.010(12)	120(11)
Ow41–H41A···O43	0.961(12)	1.84(3)	2.716(6)	151(5)
Ow41–H41B···O64	0.963(12)	2.05(3)	2.912(5)	148(4)
Ow42–H42A···O82^{IX}	0.961(12)	1.81(2)	2.752(6)	166(5)
Ow42–H42B···O84^{X}	0.953(12)	1.88(3)	2.791(5)	159(6)

[a]Symmetry codes: I, $1 - x$, $1 - y$, $-z$; II, x, $\frac{1}{2} - y$, $-\frac{1}{2} + z$; III, $1 - x$, $-y$, $-z$; IV, x, $\frac{2}{3} - y$, $\frac{1}{2} + z$; V, $1 - x$, $\frac{1}{2} + y$, $\frac{1}{2} - z$, VI, $2 - x$, $\frac{1}{2} + y$, $\frac{1}{2} - z$; VII, $2 - x$, $1 - y$, $-z$; VIII, $2 - x$, $2 - y$, $-z$; IX, $2 - x$, $-\frac{1}{2} + y$, $\frac{1}{2} - z$; X, x, $-1 + y$, z.

Table 4 Selected bond distances (Å) and angles (°) in $La_2(H_2O)_2(C_2H_{10}N_2)_3(SO_4)_6{\cdot}4H_2O$, **2**

Within La polyhedra			
La–O13	2.411(4)	La–O31	2.473(3)
La–O21	2.598(4)	La–O32	2.579(3)
La–O22	2.600(4)	La–O33	2.581(3)
La–O23	2.604(4)	La–Ow1	2.533(4)
La–O24	2.573(4)		
Within ethylenediammonium ions[a]			
N1–C1	1.474(8)	N1–C1–C2	111.0(5)
C1–C2	1.494(9)	N2–C2–C1	111.1(6)
C2–N2	1.480(8)		
N3–C3	1.490(8)	N3–C3–C3	110.1(6)
C3–C3[I]	1.49(1)		

[a]Symmetry code: I, $-x$, $1-y$, $1-z$.

selected with a diffracted-beam graphite monochromator. The powdered samples were placed in an Anton Paar HTK1200 high-temperature oven camera. The data were collected in air over the angular range 5–90° (2θ) (step length 0.02° 2θ, counting times 55/15/15 s step^{-1}) for $La_2(C_4H_{12}N_2)(SO_4)_4{\cdot}0.5H_2O$, $La_2(C_4H_{12}N_2)(SO_4)_4$ and $La_2(C_2H_{10}N_2)_3(SO_4)_6{\cdot}2H_2O$.

The extraction of peak positions for indexing was carried out with the Socabim fitting program, available in the PC software package DIFFRACplus supplied by Bruker AXS. Pattern indexing was carried out by means of the program DICVOL91.[26]

Thermal analyses

Temperature dependent X-ray diffraction (TDXD) was performed with a powder diffractometer combining the curved-position-sensitive detector (CPS120) from INEL and a high temperature attachment from Rigaku. The detector was used in a semi-focusing geometry by reflection with the monochromatic Cu Kα_1 radiation, as described elsewhere.[27] In this geometry the flat sample is stationary. An angle of 6° between the incident beam and the surface of the sample was selected. Due to the stationary sample, preferred orientation effects can be strongly enhanced, in case of micro-crystals present in the powder, for *hkl* planes (and their higher orders) having Bragg angles in the vicinity of the incident angle of the beam. This effect can appear suddenly if there are slight changes in the position of the micro-crystals due, for instance, to the heating process or to phase transformations.[27] The thermal decomposition of the two compounds $La_2(H_2O)_2(C_4H_{12}N_2)(SO_4)_4$, **1**, and $La_2(H_2O)_2(C_2H_{10}N_2)_3(SO_4)_6{\cdot}4H_2O$, **2**, were carried out under flowing air.

Thermogravimetric (TG) measurements were performed with a Rigaku Thermoflex instrument under flowing air. The powdered samples were spread evenly in a large platinum crucible to avoid mass effects.

The analysis of the gas evolved from the solids in the course of their thermal decomposition was carried out by using a Varian 311 mass spectrometer. Small amounts of the samples, initially ground, were placed in a reaction chamber near the ionisation source under vacuum and heated gradually until 400 °C.

Results

Description of the structures

The structures of $La_2(H_2O)_2(C_4H_{12}N_2)(SO_4)_4$, **1**, and $La_2(H_2O)_2(C_2H_{10}N_2)_3(SO_4)_6{\cdot}4H_2O$, **2** consist both of inorganic anionic frameworks, $[La_2(H_2O)_2(SO_4)_4]^{2-}$ for **1** and $[La_2(H_2O)_2(SO_4)_6]^{6-}$ for **2**, charge-compensated by the piperazinium and ethylenediammonium cations located in accessible voids, together with additional water molecules in **2**. Compound **1** exhibits a three-dimensional architecture (Fig. 1), while **2** has clearly a layered-type structure (Fig. 2). The frameworks are built from one ten-fold and three nine-fold coordinated lanthanum atoms for **1** and one nine-fold coordinated lanthanum atom for **2**, connected through the corners or the vertices by sulfate tetrahedra, which ensure the propagation of the network, and by water molecules to complete the coordination sphere. In compound **1**, the lanthanum atoms are surrounded as follows: for La1, four bidentate and two monodentate sulfate anions; for La2, three bidentate and three monodentate sulfate groups; for La3 and La4, one bidentate and five monodentate sulfate tetrahedra, and two water molecules (Table 2). In compound **2**, the lanthanum atom is surrounded by three bidentate and two monodentate sulfate groups and one water molecule (Table 4). In **1**, the La–O distances fall into the spread range 2.431(7)–2.881(3) Å (Table 2) [mean distance, 2.587(4) Å], with average distances

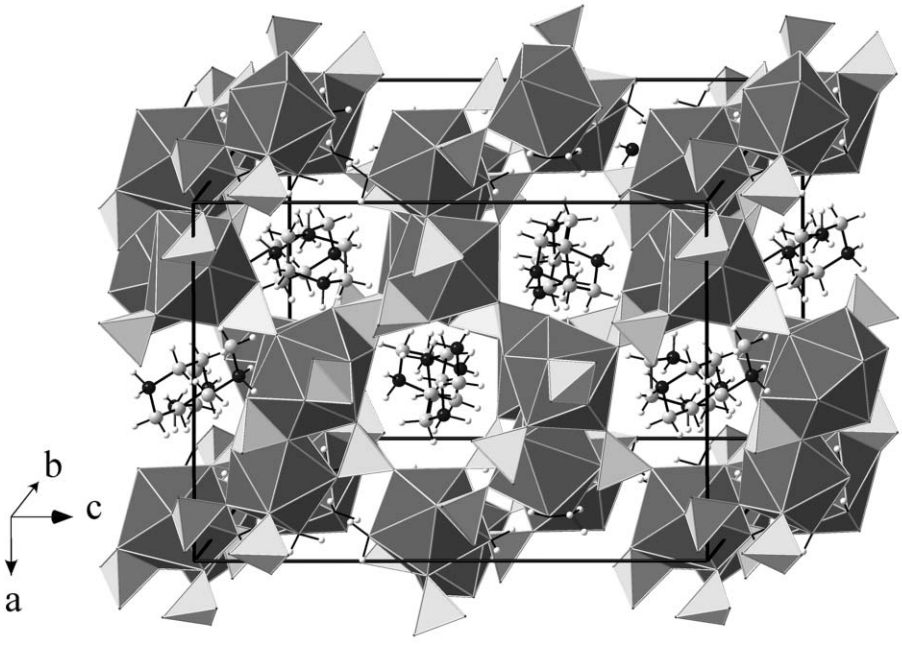

Fig. 1 Crystal structure of $La_2(H_2O)_2(C_4H_{12}N_2)_2(SO_4)_4$, **1**, showing the three-dimensional arrangement of lanthanum polyhedra (dark grey) and sulfate tetrahedra (light grey). The piperazinium cations are located inside the cavities (C: light grey circle, N: black circle, H: small white circle).

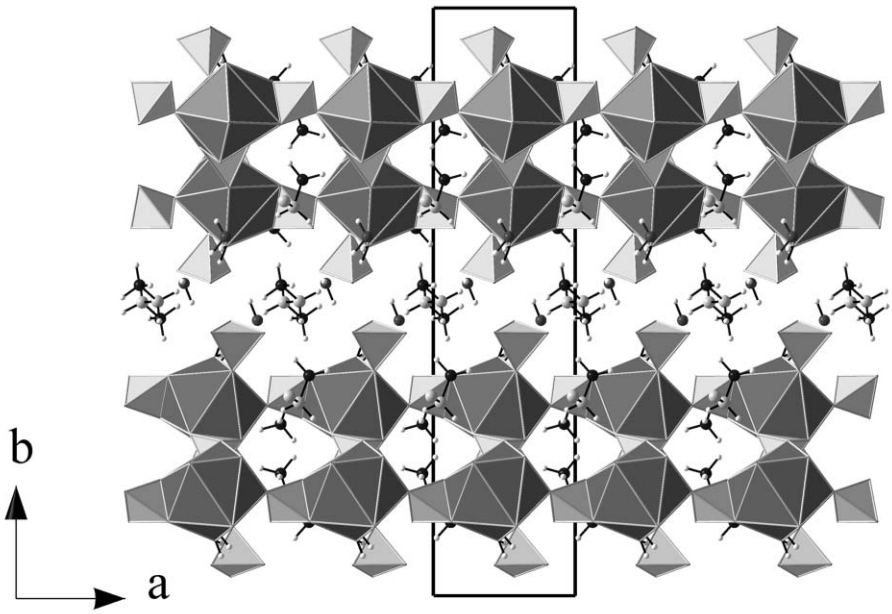

Fig. 2 Projection of the layered structure of $La_2(H_2O)_2(C_2H_{10}N_2)_3(SO_4)_6{\cdot}4H_2O$, **2**, along the *c* axis. Lanthanum polyhedra: dark grey, sulfate tetrahedra: light grey, Ow: grey circle, C: light grey circle, N: black circle, H: small white circle.

of 2.655(3) Å for the ten-fold coordinated lanthanum atom and 2.564(4) Å for the nine-fold coordinated lanthanum atoms. In **2**, the La–O distances vary in the narrower range 2.411(4)–2.604(4) Å (Table 4) [average distance, 2.550(4) Å]. These values are in agreement with those calculated with the program VALENCE,[28] *i.e.* 2.617 Å and 2.579 Å for ten-fold and nine-fold coordinated lanthanum atoms, respectively, and those reported in the literature, *i.e.* 2.53(3)–2.90(4) Å obtained from powder diffraction data for β-$(NH_4)La(SO_4)_2$[12] and 2.480(8)–2.801(8) Å for $CsLa(SO_4)_2$.[29] It should be noted that the elongated La–O bonds in **1** correspond to O atoms bridging two lanthanum atoms, *i.e.* O21, O23 and O83 (see Table 2).

There are only small variations in S–O bond lengths which are between 1.433(4) Å and 1.496(4) Å (except for the split oxygen atoms O33 and O34), with an average value of 1.468(4) Å, in **1** and between 1.445(4) Å and 1.491(4) Å, with an average value of 1.474(4) Å, in **2**. These values are in agreement with those commonly observed in metal sulfates.[9] In the same way, the O–S–O angles range from 104.9(2)° to 112.9(2)° in **1** and from 105.4(2)° to 111.6(2)° in **2**, which are close to the theoretical value of a tetrahedral angle. In both compounds, sulfate oxygen atoms are not all connected to the lanthanum atoms. In **1**, only O43 and O82 (over 32 sulfate O atoms in the asymmetric unit) point towards the cavities and form hydrogen bonds with two water molecules and a piperazinium N atom (Table 3). In the layered compound **2**, four sulfate O atoms (over 12 in the asymmetric unit) are not bonded to the lanthanum atoms and point towards the interlayer space. An interesting feature is that three O atoms belong to only one sulfate group, *i.e.* O11, O12 and O14, which leads the base of the tetrahedron $S1O_4$ to define the frontier of the inorganic sheet. The fourth non-bonded sulfate O atom, O34, points outwards from the vacant space generated by the corrugation of the layer. All of them form hydrogen bonds with either water molecules or ethylenediammonium N atoms (Table 5 and Fig. 3).

In compound **1**, the piperazine molecules are located in cavities with 8-ring apertures (Fig. 1). The first ring is similar, in shape and size, to that observed in zeolite ZK-5,[30] *i.e.* a free diameter of 3.9 Å, and in $Ga_5(PO_4)_5F_4{\cdot}2[N_2C_4H_{12}]$.[31] The second 8-ring is highly distorted and displays a critical dimension of 5.2 × 2.1 Å. It is comparable with 8-ring systems encountered in natural zeolites, *e.g.*, in brewsterite (5.0 × 2.3 Å).[30]

Table 5 Possible hydrogen bonds (Å) in $La_2(H_2O)_2(C_2H_{10}N_2)_3(SO_4)_6{\cdot}4H_2O$, **2**

D–H···A[a]	*d*(D–H)	*d*(H···A)	*d*(D···A)	∠D–H···A/°
Ow1–H11···Ow3^{I}	0.95(2)	2.30(4)	3.17(1)	153(6)
Ow1–H12···O14	0.95(2)	1.75(3)	2.681(6)	165(7)
Ow2–H21···O12^{II}	0.96(2)	1.84(3)	2.785(7)	170(10)
Ow2–H22···O11^{III}	0.95(2)	1.84(4)	2.759(7)	162(9)
Ow3–H31···Ow2^{IV}	0.95(2)	1.93(4)	2.856(8)	162(9)
Ow3–H32···O22^{V}	0.95(2)	2.11(6)	2.896(7)	140(7)
N1–HN1A···O12^{II}	0.98(2)	1.88(2)	2.846(7)	173(5)
N1–HN1B···Ow3^{VI}	0.98(2)	1.92(3)	2.884(9)	166(7)
N1–HN1C···O33^{VI}	0.98(2)	2.12(2)	3.095(7)	172(7)
N2–HN2A···O32^{VII}	0.97(2)	2.13(4)	3.000(7)	148(5)
N2–HN2B···O24^{VIII}	0.98(2)	2.14(5)	2.966(6)	140(6)
N2–HN2C···O21^{IX}	0.98(2)	1.99(2)	2.971(6)	177(6)
N3–HN3A···O14^{X}	0.97(2)	1.87(2)	2.840(6)	178(7)
N3–HN3B···O34^{XI}	0.96(2)	2.31(5)	2.977(7)	126(5)
N3–HN3C···Ow2^{VIII}	0.97(2)	1.85(4)	2.755(8)	155(6)

[a]Symmetry codes: I, *x*, *y*, −1 + *z*; II, 1 − *x*, ½ + *y*, ⅔ − *z*; III, *x*, ½ − *y*, ½ + *z*; IV, 1 − *x*, −½ + *y*, ⅔ − *z*; V, *x*, *y*, 1 + *z*; VI, −*x*, ½ + *y*, ⅔ − *z*; VII, −*x*, ½ + *y*, ½ − *z*; VIII, −*x*, 1 − *y*, 1 − *z*; IX, 1 − *x*, 1 − *y*, 1 − *z*; X, 1 − *x*, ½ + *y*, ½ − *z*; XI, −1 + *x*, ½ − *y*, ½ + *z*.

The size of the voids was analysed using the program PLATON.[32] The organic part of the structure was omitted for calculations. The vacant spaces, which contain the piperazinium cations, have a space-filling volume of 204 Å^3. This result is in agreement with the volume occupied by one piperazine group, which would approximate the molecular volume of piperazine to be 164 ± 5 Å^3. Furthermore, the piperazinium groups are strongly hydrogen-bonded to the oxygen atoms of the anionic framework as shown in Fig. 4 and Table 3. Hence, there is a strong templating effect of the diprotonated piperazine, as found in sodalite analogs[33] for example.

In contrast to the piperazine templated compound **1**, the ethylenediammonium cations are located in the free vacancies arising from the corrugated layered structure of compound **2** (Fig. 3). They adopt a staggered conformation with a dihedral angle of 177.5° for N1–C1–C2–N2 and strictly 180° for N3–C3–C3–N3 due to the location of the group on the symmetry centre. They strongly interact with the sulfate groups and the non-coordinated water molecules *via* hydrogen bonds (Table 5

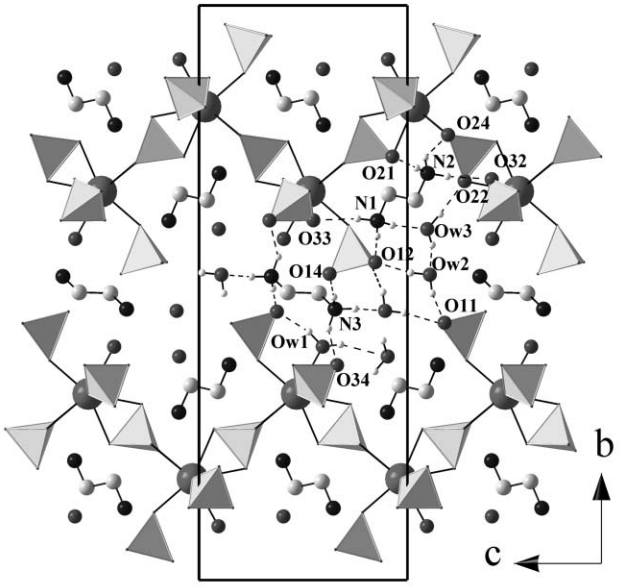

Fig. 3 Projection of the structure of $La_2(H_2O)_2(C_2H_{10}N_2)_3(SO_4)_6{\cdot}4H_2O$, **2**, along the *a* axis, showing the corrugation of the inorganic sheets and the location of ethylenediammonium cations and water molecules. The hydrogen bonding scheme is shown in part of the structure. Hydrogen bonds are represented by the dotted lines. H atoms have been partially omitted for clarity.

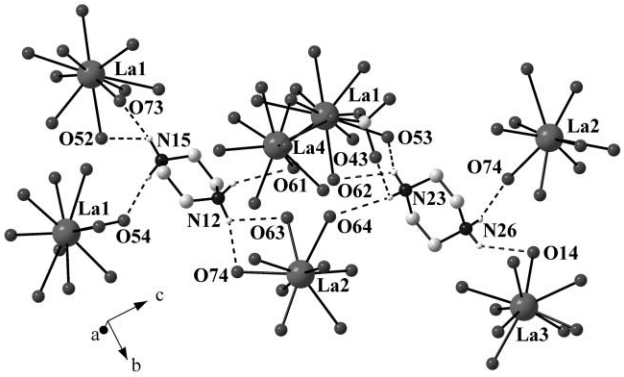

Fig. 4 Partial representation of the hydrogen bonds in $La_2(H_2O)_2(C_4H_{12}N_2)_2(SO_4)_4$, **1**, showing the interactions between the piperazinium cations and the framework oxygen atoms.

and Fig. 3). The layered structure of **2** can be compared to those of β-$(NH_4)La(SO_4)_2$[12] and of $(N_2H_5)Nd(H_2O)(SO_4)_2$,[34] except that for the latter the hydrazinium groups are connected to the Nd atom. These compounds are built up from corrugated anionic chains of rare-earth sulfates, stabilised with the organic entities in the interlayer space *via* hydrogen bonds. Fig. 5 shows that the distance between the mean planes of two adjacent inorganic sheets dramatically increases according to the presence of ammonium (4.50 Å), hydrazinium (7.88 Å) and ethylenediammonium (13.35 Å) cations in the interlayer space. For the last compound, **2**, the mean interlayer distance corresponds to a small distance between the two closest La atoms, *i.e.* 9.40 Å, and a long distance between the two farthest La atoms, *i.e.* 17.30 Å, projected onto the *bc* plane. However, the shortest O–O distance between two adjacent layers is almost the same in the three compounds, *i.e.* about 3.10 Å in the ammonium and hydrazinium compounds and about 3.02 Å between O14 and its symmetry equivalent atom lying in $(-x, -y, -z)$ in **2**. This observation might explain the strong deformation of the inorganic sheets in **2** when introducing longer organic chains in the interlayer space.

Thermal decomposition

$La_2(H_2O)_2(C_4H_{12}N_2)(SO_4)_4$. Temperature-dependent X-ray diffraction (Fig. 6) and thermogravimetric analysis (Fig. 7) of lanthanum piperazinium sulfate, **1**, reveal that the dehydration starts at 130 °C and proceeds through two stages. A loss of 1.5 water molecules is obtained in the range 130–160 °C (observed weight loss 3.4%). This corresponds to a noticeable change in the diffraction patterns, as seen in Fig. 6. (It should be noted here that the fluctuation of some line intensities in the pattern of the precursor arises from residual micro-crystals remaining in the powder after grinding, as explained in the Experimental section; additional *in situ* diffraction patterns collected with a $\theta/2\theta$ mode clearly showed the stability of the precursor until 130 °C. The fluctuations disappear after the first chemical transformation as a consequence of the uniform fragmentation of all precursor grains.) According to the TDXD plot and the TG curve, the hemihydrated phase is stable until 230 °C. The departure of the remaining $0.5H_2O$ involves a few modifications of the diffraction lines. Powder diffraction patterns of $La_2(C_4H_{12}N_2)(SO_4)_4{\cdot}0.5H_2O$ and $La_2(C_4H_{12}N_2)(SO_4)_4$ could be obtained *in situ* at 160 °C and 270 °C, respectively. Although the two phases are not well crystallised, the indexing of the patterns could be carried out from the 17 first well-resolved diffraction lines. For $La_2(C_4H_{12}N_2)(SO_4)_4{\cdot}0.5H_2O$, a monoclinic solution was found, with unit cell dimensions a = 16.210(9) Å, b = 9.139(6) Å, c = 23.41(2) Å, β = 107.96(6)°, V = 3299(3) Å^3 [M_{17} = 29, F_{17} = 71(0.006,40)]. The systematic absences were found consistent with the space group $P2_1/n$. For the anhydrous phase, a comparable solution was found, with unit cell parameters a = 16.418(7) Å, b = 9.274(3) Å, c = 23.30(1) Å, β = 108.27(4)°, V = 3369(1) Å^3 [M_{17} = 27, F_{17} = 62(0.006,46)]. The systematic absences were also found consistent with the space group $P2_1/n$. There are strong analogies

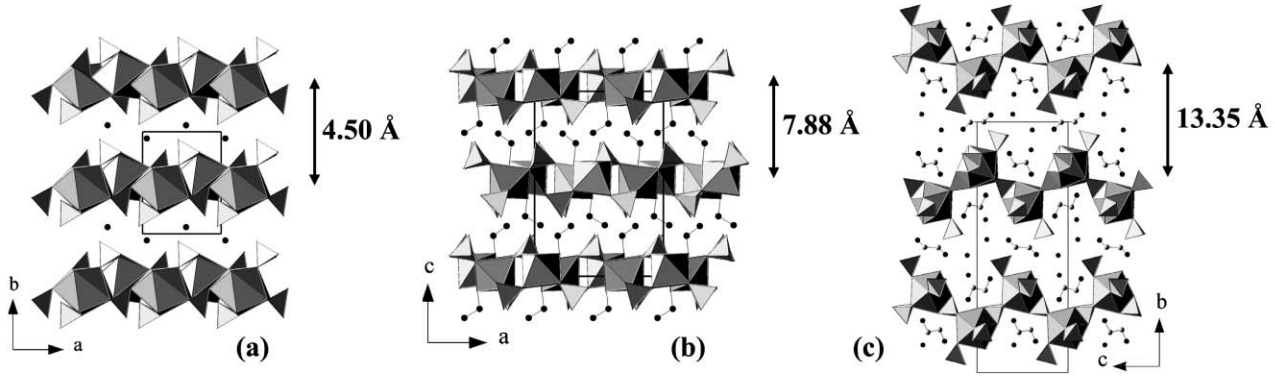

Fig. 5 Representation of the crystal structures of (a) β-$(NH_4)La(SO_4)_2$, (b) $(N_2H_5)Nd(H_2O)(SO_4)_2$, (c) $La_2(H_2O)_2(C_2H_{10}N_2)_3(SO_4)_6{\cdot}4H_2O$, **2**.

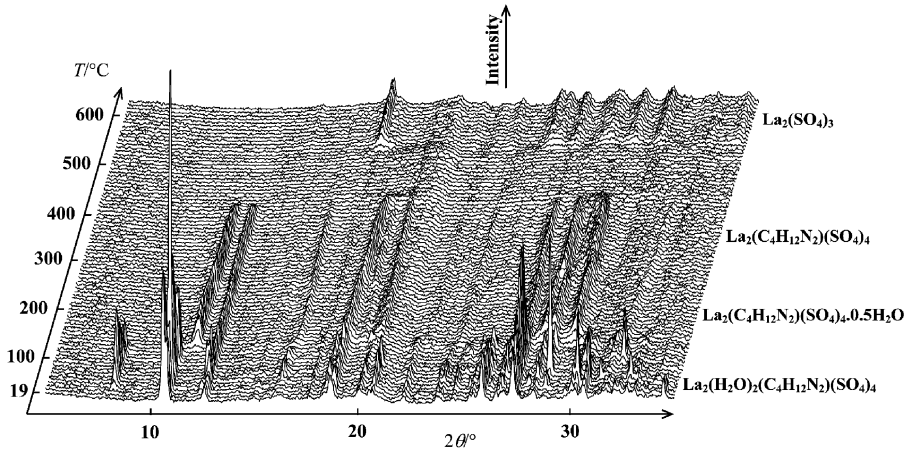

Fig. 6 TDXD plot for the decomposition of $La_2(H_2O)_2(C_4H_{12}N_2)_2(SO_4)_4$, **1**, in air (5 °C h^{-1}, counting time of 5400 s per pattern).

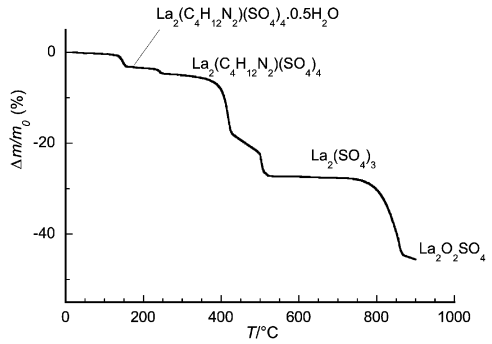

Fig. 7 TG curve for the decomposition of $La_2(H_2O)_2(C_4H_{12}N_2)_2(SO_4)_4$, **1**, in air (5 °C h^{-1}).

between the unit cell parameters of the two phases and that of the precursor **1**, despite the change of space group from $P2_1/c$ to $P2_1/n$ upon dehydration. It is interesting to note that the departure of the first $1.5H_2O$ is in agreement with the contraction of the unit cell, while an expansion of 2% of the cell volume is involved during the release of the remaining 0.5 water molecule.

The anhydrous compound appears stable in the TDXD plot until around 400 °C, although the line intensities decrease from ~370 °C. In fact the TG curve shows a continuous weight loss from 230 to ~360 °C and, then, a rapid loss until 530 °C, which is associated with an amorphous state in the TDXD plot (Fig. 6). At this temperature, the total weight loss reaches 27.3%. This corresponds to the formation of $La_2(SO_4)_3$, as observed on the TDXD plot (ICDD file No. 45-0904). The high decomposition temperature of the piperazine group is not surprising, due to the fact that the molecule is occluded in the cavities and is strongly hydrogen bonded to the framework (Fig. 4). Such a high temperature (390 °C) has also been observed recently for the decomposition of piperazine sulfate.[35] The final stage of the decomposition starts at 725 °C and leads to $La_2O_2SO_4$, identified from its diffraction pattern (observed weight loss at 900 °C, 45.6% ; calculated weight loss, 48.2%).

$La_2(H_2O)_2(C_2H_{10}N_2)_3(SO_4)_6{\cdot}4H_2O$. The results of thermodiffractometry and TG analyses are shown in Figs. 8 and 9, respectively. They demonstrate that the thermal decomposition of **2** proceeds through several stages. The first one occurs in the temperature range 45–55 °C and corresponds to the release of $2.6H_2O$ on the TG curve (observed weight loss, 4.1%). It is characterised by a structural modification as seen in the TDXD plot. This phase appears stable until 150 °C, while at the same time, the TG curve shows the release of 1.4 supplementary water molecules and leads to a dihydrated compound. It may be supposed at this stage that the intermediate phase contains two strongly bonded water molecules and that $1.4H_2O$ are weakly bonded to the structure and release without any structural modification. A powder X-ray diffraction pattern of this phase, which can be denoted $La_2(C_2H_{10}N_2)_3(SO_4)_6{\cdot}(2+x)H_2O$ ($0 \leqslant x \leqslant 1.4$), has been obtained *in situ* under static air at 62 °C. Indexing of the pattern from the first 20 diffraction lines with an absolute error of 0.03° (2θ) led to a monoclinic solution with unit cell dimensions $a = 6.706(2)$ Å, $b = 25.139(3)$ Å, $c = 9.818(2)$ Å, $\beta = 100.80(2)°$, $V = 1625.8(5)$ Å^3 [$M_{20} = 31$, $F_{30} = 41(0.009,83)$]. From the analysis of the indexed powder data

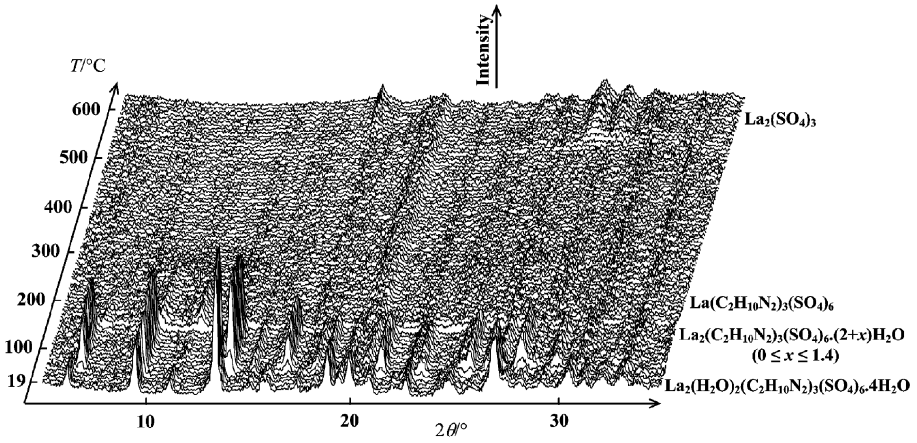

Fig. 8 TDXD plot for the decomposition of $La_2(H_2O)_2(C_2H_{10}N_2)_3(SO_4)_6{\cdot}4H_2O$, **2**, in air (15 °C h^{-1}, counting time of 1800 s per pattern).

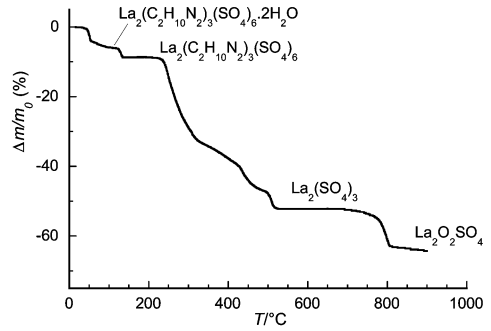

Fig. 9 TG curve for the decomposition of $La_2(H_2O)_2(C_2H_{10}N_2)_3(SO_4)_6{\cdot}4H_2O$, **2**, in air (10 °C h^{-1}).

the systematic absences were found consistent with the space groups $P2_1/m$ and $P2_1$. Compared to the unit cell parameters of the precursor **2**, the departure of the first two water molecules leads to a contraction of the *b* and *c* axes and a slight distortion of the monoclinic cell (from 104.874(1)° to 100.80(2)° for β), which are responsible for the change of space group. Attempts to solve the structure of the dihydrated phase were unsuccessful, mainly because of the severe diffraction line overlap arising from peak broadening, aggravated by the lower instrument resolution due to the use of the Cu Kα doublet.

The departure of the last two water molecules, likely those coordinated to La atoms, proceeds rapidly between 150 and 165 °C and leads to an anhydrous compound, which appears to be poorly crystalline in the TDXD plot, and subsequently to an amorphous state to X-rays between 250 and 530 °C. On the TG curve (Fig. 9) it is seen that the decomposition of the anhydrous phase starts at 220 °C and that several inflections are observed, which can be attributed to the decomposition of the ethylenediammonium cations and one sulfate group. This is confirmed from the analysis of emitted gas from mass spectrometry studies, *i.e.* H_2O, NH_3, CH_2NH_2, SO_2 and SO_3. It is obvious that decomposition under vacuum proceeds in superimposed stages, so that a decomposition scheme cannot be proposed. The end of the decomposition at 530 °C is marked by a plateau corresponding to a total weight loss of 52.2% and the crystallisation of a product, which has been identified from diffraction as $La_2(SO_4)_3$ (theoretical weight loss, 50.6%). The final stage corresponds to the decomposition of the sulfate salt between 690 and 810 °C into $La_2O_2SO_4$ (observed weight loss at 810 °C, 64.2%; expected weight loss, 67.6%).

Conclusion

The two new compounds described in this study confirm the possibility of synthesising new sulfate-based inorganic materials by utilising structure-directing amines. The phases reported present different topologies, *i.e.* 3D and 2D crystal structures which are likely generated by the steric effects associated with a cyclic conformation in the case of piperazine and a linear feature for ethylenediamine. It must be noted that, again, similarities are observed between the layered structure reported for a lanthanum ammonium phase and the compound reported here for the smallest amine, *i.e.* the lanthanum sulfate ethylenediamine. The thermal stability of the organic group is also clearly understood from the position of the cation in the structure, namely the framework remains stable at higher temperatures in the case of the occluded piperazine, while it is less stable in the case of the ethylenediamine layered structure. The results reported here give confidence in the possibility of preparing new sulfate-based materials in the presence of amines with varied structure topologies.

Acknowledgements

The authors thank Dr T. Roisnel (Centre de Diffractométrie X, Université de Rennes I) and Mr G. Marsolier for their assistance in the single-crystal and powder X-ray diffraction data collection, respectively, and they are grateful to Dr P. Guénot (CRMPO, Université de Rennes I) for the mass spectrometry analyses.

References

1 A. K. Cheetham, G. Férey and T. Loiseau, *Angew. Chem. Int. Ed.*, 1999, **38**, 3268–3292.
2 D. J. Chesnut, D. Hagrman, P. J. Zapf, R. P. Hammond, R. LaDuca, Jr., R. C. Haushalter and J. Zubieta, *Coord. Chem. Rev.*, 1999, **190–192**, 737–769.
3 S. T. Wilson, B. M. Lok, C. A. Messina, T. R. Cannan and E. M. Flanigen, *J. Am. Chem. Soc.*, 1982, **104**, 1146–1147.
4 C. N. R. Rao, S. Natarajan, A. Choudhury, S. Neeraj and A. A. Ayi, *Acc. Chem. Res.*, 2001, **34**, 80–87.
5 T. Conradsson, M. S. Dadachov and X. D. Zou, *Microporous Mesoporous Mater.*, 2000, **41**, 183–191.
6 B. A. Reisner, A. Tripathi and J. B. Parise, *J. Mater. Chem.*, 2001, **11**, 887–890.
7 S. Ekambaram and S. C. Sevov, *Inorg. Chem.*, 2000, **39**, 2405–2410 and references therein.
8 M. S. Wickleder, *Chem. Rev.*, 2002, **102**, 2011–2087.
9 D. Louër, J. Rius, P. Bénard-Rocherullé and M. Louër, *Powder Diffr.*, 2001, **16**, 86–91 and references therein.
10 B. Eriksson, L. O. Larsson, L. Niinistö and U. Skoglund, *Inorg. Chem.*, 1974, **13**, 290–295.
11 N. L. Sarukhanian, L. D. Iskhakova and V. K. Trunov, *Kristallografiya*, 1984, **29**, 435–439.
12 P. Bénard-Rocherullé, H. Tronel and D. Louër, *Powder Diffr.*, 2002, **17**, 210—217.
13 L. Niinistö, J. Toivonen and J. Valkonen, *Finn. Chem. Lett.*, 1980, **3**, 87–92.
14 H. Tronel, DEA Report, Université de Rennes I, France, 1999.
15 C. N. Morimoto and E. C. Lingafelter, *Acta Crystallogr., Sect. B*, 1970, **26**, 335–341.
16 A. Choudhury, J. Krishnamoorthy and C. N. R. Rao, *Chem. Commun.*, 2001, 2610–2611.
17 I. Bull, P. S. Wheatley, P. Lightfoot, R. E. Morris, E. Sastre and P. A. Wright, *Chem. Commun.*, 2002, 1180–1181.
18 N. Audebrand, M.-L. Vaillant, J.-P. Auffrédic and D. Louër, *Solid State Sci.*, 2001, **3**, 483–494.
19 S. Ayyappan, A. K. Cheetham, S. Natarajan and C. N. R. Rao, *Chem. Mater.*, 1998, **10**, 3746–3755.
20 E. Jeanneau, N. Audebrand and D. Louër, *Chem. Mater.*, 2002, **14**, 1187–1194.
21 Nonius, *Kappa CCD Program Software*, Nonius BV, Delft, The Netherlands, 1998.
22 Z. Otwinowski and W. Minor, *Methods Enzymol.*, 1997, **276**, 307–326.
23 P. Coppens, in *Crystallographic Computing*, ed. F. R. Ahmed, S. R. Hall and C. P. Huber, Munksgaard, Copenhagen, 1970, pp. 255–270.
24 A. Altomare, M. C. Burla, M. Camalli, G. L. Cascarano, C. Giacovazzo, A. Guagliardi, A. G. G. Moliterni, G. Polidori and R. Spagna, *J. Appl. Crystallogr.*, 1999, **32**, 115–119.
25 G. M. Sheldrick, *SHELXL-97: Program for Crystal Structure Refinement*, University of Göttingen, Germany, 1997.
26 A. Boultif and D. Louër, *J. Appl. Crystallogr.*, 1991, **24**, 987–993.
27 J. Plévert, J.-P. Auffrédic, M. Louër and D. Louër, *J. Mater. Sci.*, 1989, **24**, 1913–1918.
28 I. D. Brown, *J. Appl. Crystallogr.*, 1996, **29**, 479–480.
29 N. Bukovec, V. Kaucic and L. Golic, *Acta Crystallogr., Sect. B*, 1980, **36**, 129–130.
30 *Atlas of Zeolite Framework Types*, ed. C. Baerlocher, W. M. Meier and D. H. Olson, Elsevier, Amsterdam, 5th revised edn., 2001.
31 F. Bonhomme, S. G. Thoma, M. A. Rodriguez and T. M. Nenoff, *Microporous Mesoporous Mater.*, 2001, **47**, 185–194.
32 A. L. Spek, *Acta Crystallogr., Sect. A*, 1990, **46**, C-34.
33 X. Bu, T. E. Gier, P. Feng and G. D. Stucky, *Microporous Mesoporous Mater.*, 1998, **20**, 371–379.
34 S. Govindarajan, K. C. Patil, H. Manohar and P.-E. Werner, *J. Chem. Soc., Dalton Trans.*, 1986, 119–123.
35 K. Jayaraman, A. Choudhury and C. N. R. Rao, *Solid State Sci.*, 2002, **4**, 413–422.